International Journal of Biological Macromolecules 308 (2025) 142552

Contents lists available at ScienceDirect

International Journal of Biological Macromolecules

journal homepage: www.elsevier.com/locate/ijbiomac

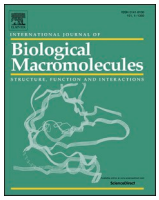

Fabrication of pullulan-chitosan fiber membranes for enhanced hemostatic applications

Jefferson Reinoza [a], Rahul Tiwari [b], Isabela Morales [a], Luis Sotelo [a], Debabrata Sengupta [a], Juan Pablo Hernandez [a], Victoria Padilla [a], Murali M. Yallapu [b,*], Karen Lozano [a,c,**]

[a] Center for Nano Technology/College of Engineering and Computer Science, University of Texas Rio Grande Valley (UTRGV), Edinburg, TX 78539, USA
[b] Division of Cancer immunology and Microbiology, South Texas Center of Excellence in Cancer Research, Medicine and Oncology Integrated Service Unit, School of Medicine, University of Texas Rio Grande Valley (UTRGV), McAllen, TX 78504, USA
[c] Materials Science & Nanoengineering, Rice University, George R. Brown School of Engineering and Computing, Houston, TX 77005, USA

ARTICLE INFO

Keywords:
Forcespinning
Nanofibers
Hemostasis
Chitosan
Pullulan

ABSTRACT

Pullulan-based fibers blended with chitosan (Chi) were developed using a rotational spinning method for potential biomedical applications. Aqueous precursor formulations containing 15 % by weight in pullulan and varying Chi concentrations (6 % and 7 %) were optimized to produce nanofibers at elevated temperatures and rotational speeds exceeding 7 k rpm. The highest fiber production yields of approximately 90 % and 65 % were achieved at 13 k rpm for the 6 % and 7 % Chi formulations, respectively. The pullulan-chitosan fibers were characterized by scanning electron microscopy, Fourier transform infrared spectroscopy, dynamic mechanical analyzer, powder X-ray diffraction, and rheological property measurements. Morphological analyses revealed nanometric fiber diameters and a decrease in bead formation with increasing rotational speeds. Thermal stability studies, conducted via thermogravimetric and differential thermal analyses, showed that the composite fibers exhibited intermediate degradation behaviors between their individual polymer components, indicating good integration of Chi into the pullulan matrix. Elemental analysis confirmed the successful incorporation of Chi into the fibers, with nitrogen content closely matching theoretical predictions. Functional assessments demonstrated the hemocompatibility of the Pull-Chi fibers with hemolysis rates below 1 %. Additionally, the fibers exhibited superior hemostatic potential, effectively promoting blood clotting in vitro testing. These findings underscore the promise of Pull-Chi fibers as multifunctional biomaterials for applications in wound healing and tissue engineering. Future studies involving animal models are warranted to validate their clinical potential.

1. Introduction

According to statistical data from the National Trauma Institute in the United States (US), trauma remains the leading cause of mortality among individuals aged 1 to 46 Years [1]. Uncontrolled hemorrhage is a significant contributor, responsible for 60,000 deaths annually in the US alone, with an estimated 1.5 million deaths worldwide each year. This situation is further complicated by the fact that the median time from hemorrhagic shock onset to death is only approximately 2 h, underscoring the critical need for immediate intervention to improve survival outcomes. The urgency of developing effective hemorrhage control methods is especially pronounced in military settings [2,3].

To control bleeding, common, and standardized methods include applying direct pressure to the bleeding site with sterile gauze or clean cloth, using a tourniquet to reduce blood flow in an extremity, or applying firm pressure on strategic points such as the femoral or the brachial artery. However, these techniques have limitations, as they may not be suitable for all body areas or in cases where a sharp object remains embedded in the wound. Currently, there are some commercial products available for bleeding control from open wounds in different areas of the body [4,5]. These products include liquids, solid powders, and bandages or dressings that can be directly applied to the wound [6]. In addition, these products also support the coagulation process, aiding the body's natural ability to stop blood loss.

* Corresponding author at: School of Medicine, University of Texas Rio Grande Valley, Room 2.249, 5300 North L Street, McAllen, TX 78504, USA
** Correspondence to: K. Lozano, Department of Materials Science and NanoEngineering, George R. Brown School of Engineering and Computing, Rice University, Houston, TX 77005, USA.
E-mail addresses: murali.yallapu@utrgv.edu (M.M. Yallapu), kl206@rice.edu (K. Lozano).

https://doi.org/10.1016/j.ijbiomac.2025.142552
Received 27 November 2024; Received in revised form 14 March 2025; Accepted 24 March 2025
Available online 26 March 2025

Nanofibers serve as an excellent platform for the controlled delivery of drugs, proteins, peptides, genes, and growth factors, making them highly suitable for wound healing and hemostatic applications. Therefore, high-throughput preparation of nanofibers has gained significant interest. Electrospinning is the most widely used process for producing nanofibers [7–9]. Various nanofiber techniques, including bubbfil spinning [10], centrifugal spinning [11], and freeze-drying [12] have demonstrated potential in biological applications. Based on polymer preparation, electrospinning can be divided into solution electrospinning and melt electrospinning. While solution electrospinning is extensively studied, its practical implementation is often hindered by limitations such as low productivity, the need for additional solvent extraction steps, and the use of hazardous solvents [13]. In contrast, melt electrospinning eliminates solvent-related concerns; however, challenges such as high polymer melt viscosity, difficulties in producing finer fibers, and electrical discharge complications associated with high-voltage applications have limited its adoption. Centrifugal spinning, also referred to as rotary spinning or rotational jet spinning, has emerged as a well-established alternative. Unlike electrospinning, this technique does not require high voltage, thereby mitigating associated safety risks. Additionally, centrifugal spinning offers enhanced production efficiency by increasing rotational speed, allowing for rapid and large-scale nanofiber synthesis. Compared to electrospinning, it enables the processing of polymers at significantly higher concentrations, leading to reduced solvent consumption and lower production costs [11,14,15]. Hammami et al. [16] demonstrated that centrifugal force spinning facilitates nanoscale fiber production, with successful fiber formation requiring polymer chain overlap or entanglement. Furthermore, they observed that nanofiber spinnability improved significantly when using needles with smaller inner diameters. Erickson et al. [17] employed a centrifugal electrospinning technique to fabricate well-aligned chitosan/polycaprolactone (PCL) nanofibers. Compared to conventional electrospinning, centrifugal electrospinning yielded nanofibers with more uniform diameters and improved vertical alignment. Notably, the nanofiber diameter distribution achieved via centrifugal electrospinning ranged from 100 nm to 275 nm, markedly narrower than the 25–450 nm range observed with traditional electrospinning [17]. These findings highlight the potential advantages of centrifugal spinning techniques in achieving precise nanofiber morphology and scalability for various biomedical applications.

Chitosan (CS) is a naturally occurring cationic polyelectrolyte copolymer derived from the deacetylation of chitin, a structural polysaccharide found in the exoskeletons of crustaceans, insects, and certain fungi. Due to its abundance as a renewable resource and its exceptional physicochemical properties, including biodegradability, biocompatibility, non-toxicity, hemostatic activity, and metal-chelating capabilities, chitosan has garnered significant interest for biomedical applications [17–20]. The electrospinning of pure chitosan has been explored using nonaqueous solvents. For instance, Ohkawa et al., [21] successfully fabricated chitosan nanofibers using trifluoroacetic acid as a solvent, with the addition of dichloromethane to enhance fiber formation [21]. Similarly, Sencadas et al., [22] increased the homogeneity of the nanofibers and methodically examined the processing parameters to provide the foundation for a reproducible method of producing chitosan nanofibers [22]. However, the environmental concerns associated with these solvent systems necessitate alternative strategies to enhance the spinnability of chitosan. One promising approach involves blending chitosan with synthetic or natural polymers to improve fiber mechanical properties and biological functionality. Synthetic polymers such as polyethylene oxide [23,24], polyvinyl alcohol [25], and polylactic acid [26] have been incorporated to enhance fiber strength and spinnability. Additionally, blending chitosan with renewable biopolymers, such as gelatin [27], alginate [28], and silk fibroin [29] have been explored to further improve biocompatibility and bioactivity. These composite nanofibers hold significant potential for various biomedical applications, including wound healing, tissue engineering, and drug delivery.

Among various biopolymers, pullulan and chitosan exhibit unique properties, including high water retention capacity, biocompatibility, biodegradability, antibacterial activity, and non-toxicity, making them promising candidates for biomedical applications [30]. Pullulan-based nanofibers have gained attention in the development of advanced wound dressing materials due to their favorable biological and physicochemical characteristics. However, despite these advantages, pullulan has inherent limitations, such as poor mechanical strength and high production costs, which can hinder its practical applications. These shortcomings can be addressed by blending pullulan with other polymers to enhance its mechanical properties and functional stability [31]. Additionally, pullulan derivatives are currently under investigation for potential biomedical applications, though they have not yet received regulatory approval for commercial use [32]. Considering the above challenges in developing cost-efficient and high-throughput nanofibers for hemostatic applications, we propose pullulan and chitosan-based nanofiber membranes. Pullulan-chitosan nanofiber system [15,33] represents a significant advancement in the development of sustainable and multifunctional materials, leveraging the synergistic properties of these biopolymers. Pullulan is a water-soluble, non-toxic, and Generally Recognized As Safe-certified polysaccharide [34]. Pullulan is produced by *Aureobasidium pullulans* and exhibits remarkable film-forming, mechanical, and adhesive characteristics. Its structural composition, consisting of maltotriose units linked via α-(1,6) and α-(1,4) glycosidic bonds, imparts flexibility and an amorphous nature, making it highly suitable for electrospinning processes [35]. Pullulan also possesses a high capacity for maintaining and regulating the many cell types that contribute to skin homeostasis. It has the potential to construct a healthy microenvironment at the injury site, allowing the wound to recover on its own while maintaining appropriate hydration [36]. Complementarily, chitosan, a deacetylated derivative of chitin, offers cationic properties, antimicrobial efficacy, and biocompatibility. The integration of these biopolymers facilitates the fabrication of electrospun nanofibers with high surface area-to-volume ratios, rendering them ideal for applications in tissue engineering, drug delivery, and wound healing [37]. This composite system exemplifies the intersection of biopolymer sustainability and functional versatility, fostering innovation in biomedical and industrial material science.

2. Materials and methods

2.1. Reagents and equipment for fiber production

Pullulan (Pull) was selected as the primary was the polymer for fiber production and procured from Tokyo Chemical Industry Co., LTD. (TCI, P0978). Chitosan (Chi), with a low molecular weight (50,000–190,000 Da, based on viscosity) and deacetylation ≥75 %, was purchased from Sigma-Aldrich. Deionized water was used as the main solvent. For the dissolution of Chi, glacial acetic acid (HAc, 99.9 %, Fisher Chemical) was used as the pH-adjusting agent. Pullulan and chitosan solutions were mixed using a Cole-Palmer 8891 sonicator to ensure homogeneity. The pH of the Pull-Chi solution was adjusted with glacial acetic acid to achieve optimal polymer solubility and compatibility. Heating was performed using an Isotemp® oven (Model 285 A, Fisher Scientific) to facilitate the fiber production process. The Pull-Chi fiber production was conducted using a Cyclone FIBERIO L-1000 M Forcespinning™ System. This homegrown equipment facilitates the centrifugal spinning of polymer solutions to produce nonwoven fibrous materials (an interior view of the equipment is depicted in Figure). The polymer solution was expelled from the spinneret through BD PrecisionGlide™ 27G x 1 ¼ needles, enabling the formation of fine fibers under high rotational speeds.

2.2. Chitosan solubility and formulation of polymeric solution

The aqueous chitosan solutions with concentrations of 6 wt% and 7

wt% were prepared by adding HAc solution. The mixed solutions were manually stirred and then subjected to ultrasonication in a sonication bath for 2 h to achieve homogeneous solutions. The solutions were left at room temperature for 18 h post-formulation to allow equilibrium and to evaluate homogeneity of the systems.

2.3. Formulation of polymeric solutions

The preparation of polymeric solutions involved dissolving chitosan in a mixture of deionized water and HAc, followed by the addition of pullulan (Pull). Initially, Chi was manually dissolved in the acid solution, Pull was then incorporated into the Chi-containing solution to form a homogenous Pull-Chi blend. The resulting solutions were subjected to ultrasonication for 2 h in a sonication bath to enhance dispersion. These solutions were subsequently injected into the spinneret of the rotational system for fiber production (See in Fig. 1). The component proportions to obtain 15 g of the formulations are presented in Table 1. A pure Pull solution was also prepared at 15 wt% in water to serve as a comparison standard with respect to the Pull-Chi formulations, this solution was acidified with an average amount of HAc used in the previous systems.

2.4. Fiber production process

Approximately 1.5 g of the prepared Pull-Chi formulations were injected into the spinneret system. The system was then preheated to 85 °C and maintained for 25 min before spinning for fiber production. Just before starting the rotational spinning process, room-temperature needles were attached to the spinneret. The spinning was conducted for a total rotation time of 20 min (10 min/cycle x2). The produced fibers were collected in two parts: a) fibers located between the vertical bus bars, used for characterization analysis, and b) all residual fibers not captured in between the vertical bars were also used to calculate production yield. A schematic representation of the Pull-Chi fiber production process is presented in Fig. 2 and Fig. 3.

2.5. Calculation of production yield

The production yield was calculated by considering both Pull and Chi as integral components of the final fiber composition. The percentages of production yields were calculated by using Eqs. 1 and 2.

$$\text{Yield } (\%) = \frac{\text{WFC}}{\text{TWPF}} \times 100 \quad (1)$$

$$\text{TWPF} = \frac{\text{FIIS}}{100} \times \text{PC} \quad (2)$$

where *WFC* is the weight of all the fiber collected (g) after each spinning process, *TWPF* is the theoretical weight of producible fibers per formulation introduced into the spinneret (g), *FIIS* is the formulation injected into the spinneret (g), and finally, *PC* corresponds to the polymer concentration (wt%) of the Pull-Chi mixture in each formulation used. Yields were calculated for F1 and F2 presented in Table 1 at different rotational velocities.

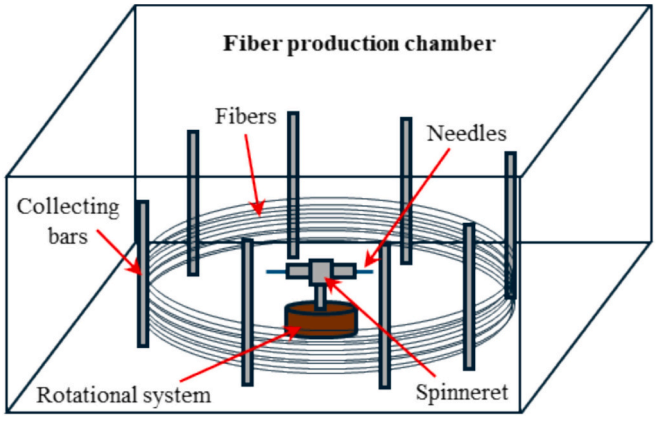

Fig. 1. Representative image of an interview of the fiber production centrifugal spinning chamber.

Table 1
Components and proportions of the Pull and Pull-Chi formulation.

Component	Comparison standard		Formulation 1 (F1)		Formulation 2 (F2)	
Pull	15 wt%	2.25 g	15 wt%	2.25 g	15 wt%	2.25 g
Chi	–	–	6 wt%	0.90 g	7 wt%	1.05 g
HAc	59 drops	0.63 g	54 drops	0.58 g	63 drops	0.68 g
Water	–	12.12 g	–	11.27 g	–	11.02 g

2.6. Characterization of fibers

The structural, morphological, thermal, and rheological properties of chitosan and pullulan powders, as well as their nanofiber samples, were comprehensively characterized using various analytical techniques.

2.6.1. Chemical characterization

The functional groups of chitosan, pullulan, and their nanofibers were analyzed using Fourier-transform infrared (FTIR) spectroscopy (Perkin Elmer, USA) equipped with a diamond-coated ZnSe crystal. Each FTIR spectrum was recorded within the wavenumber range of 4000–400 cm^{-1} at a resolution of 2 cm^{-1} based on 32 scans per sample.

2.6.2. Morphological analysis

For morphological analysis, scanning electronic microscopy (SEM) was performed using a ZEISS ΣIGMA *VP*, Gemini model. The fiber samples were sputter-coated with gold using a Denton Vacuum Desk *V* sputter coater. Images of fibers were captured at an accelerating voltage of 1 kV. Fiber diameter distribution (FDD) analysis was determined by using the ImageJ software. Elemental composition of the fibers was examined via energy-dispersive spectroscopy (EDS) using an EDAX Octane Super system (AMETEK), equipped with a 60 mm^2 active area, operating at 9–13 kV.

2.6.3. Thermal and wettability analysis

Thermal stability of the fibers was assessed using thermogravimetric analysis (TGA) on a TG 209 F3 Tarsus instrument (Netzsch). The thermal analysis was carried out under N_2 atmosphere with a flow rate of 10 mL/min. Thermal history of samples was acquired between 30 and 800 °C at a heating rate of 10 °C/min. The wettability of the nanofibers was evaluated by measuring the water contact angle (WCA) using a Kyowa contact angle meter (Model DM-1CE) at room temperature (25 °C). The Milli-Q water was used as test liquid and the equilibration time of the liquid drop was 3 s.

2.6.4. Structural and mechanical properties

The crystallinity of pullulan powders and nanofiber films was examined using X-ray diffraction (XRD) on a diffractometer (Rigaku MiniFlex600). A diffraction range of 5°-45° (2θ) was chosen. The dynamic mechanical behavior of the blends was measured by using a dynamic mechanical analyzer (DMA 242 E Artemis, Netzsch Instruments) in a dual-cantilever mode. The scanning frequency of 1 Hz and the amplitude of 10 μm were fixed, and each specimen was tested with a heating rate of 5 °C/min from −90 to 160 °C in a nitrogen atmosphere.

2.6.5. Rheological analysis

The apparent shear viscosity of spinning solutions containing different polymer concentrations of pullulan and chitosan was measured using a strain-controlled rheometer (Thermofisher Haake Mars

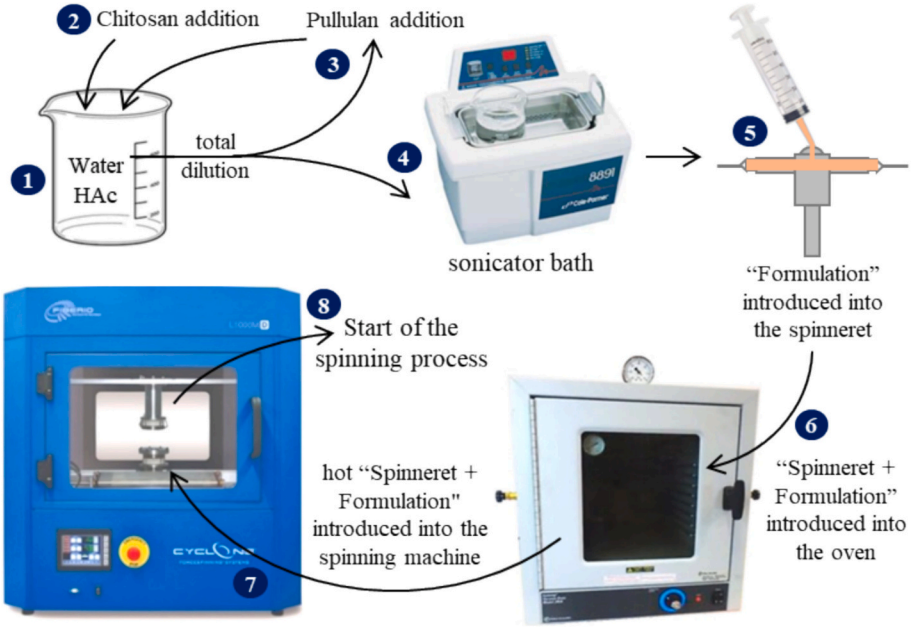

Fig. 2. General diagram of the production procedure for Pull and Pull-Chi fibers by means of the forcespinning method.

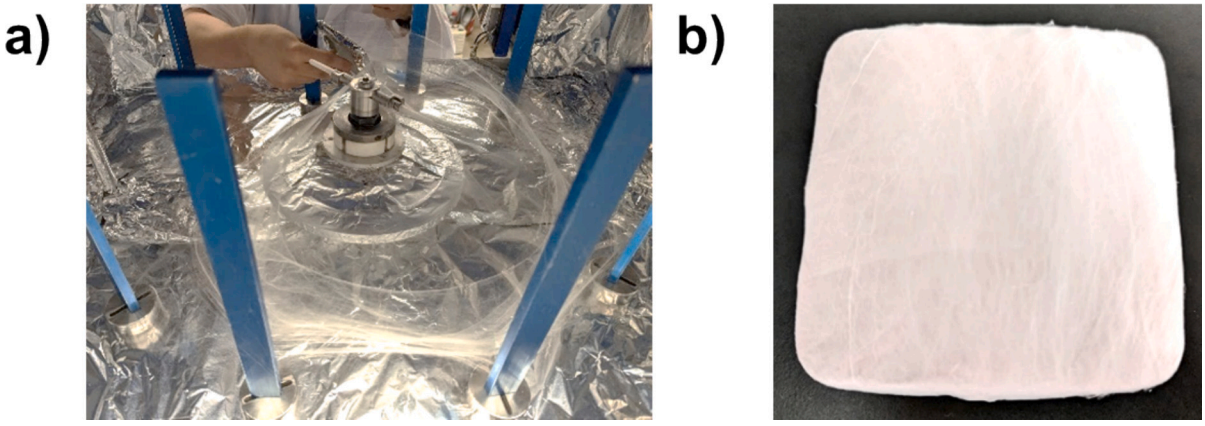

Fig. 3. Fiber production and physical image of fibers. (a) Fibers produced using pullulan and chitosan as components in aqueous solution and (b) Fibers collected between the vertical collection bars.

instrument) with cone-and-plate geometry (50 mm diameter), a gap of 0.043 mm, and a cone angle of 0.04 rad. Flow curves, depicting apparent shear viscosity versus shear rate, were recorded over a range of 0.1 to 100 s^1, at a controlled temperature of 20 °C.

2.7. Hemolytic assay

Human whole blood was procured from Zen Bio Inc. (Durham, NC). Red blood cells (RBCs) were collected by centrifuging the blood at 4 k rpm for 10 min using a 5920 R centrifuge (Eppendorf AG, Hamburg, Germany). The collected RBCs were washed and diluted 10-folds with phosphate buffered saline (PBS, 7.4 pH, 1×). For the hemolytic assay, 300 μL of the RBCs solution was further diluted with 600 μL of PBS (1×) in 1.5 mL Eppendorf tube. 2 mg of each fiber samples were incubated in 300 μL of above RBC suspension at room temperature for 2 h. In this study, PBS without fibers served as absorbance negative control ($A_{negative}$) while Triton X-100 without fibers was served as the positive control ($A_{positive}$). Following incubation, the Eppendorf tubes were centrifuged to separate RBCs, and the supernatants were collected ($A_{samaple}$). The optical density (OD) of supernatants at 544 nm was recorded using a BioTek Synergy H1 multimode reader (Agilent Technologies, USA) [38]. The percentage of hemolysis was calculated using the equation shown below.

$$\text{Hemolysis}(\%) = \frac{A_{\text{sample}} - A_{\text{negative control}}}{A_{\text{postive control}} - A_{\text{negative control}}} \times 100$$

The morphology of RBCs post-incubation was analyzed to evaluate the hemocompatibility of fibers. RBC pellets obtained after centrifugation were resuspended in 500 μL of 4 % paraformaldehyde (PFA) solution. For fixation. A 20 μL of aliquot of the fixed RBC suspension was deposited on glass slide, smeared, and covered with a cover slip. Then, morphology of RBCs was imaged on a bright-field EVOS M7000 microscope (Invitrogen, Thermo Fisher Scientific, Waltham, MA, USA) [39].

2.8. Efficiency of fibers as coagulant agents

The in vitro blood clotting index (BCI) was determined to assess the fiber's coagulant efficiency. 500 μL of whole human blood was mixed with 50 μL of 0.1 M calcium chloride solution and 20 mg of each fiber sample in a 2 mL glass vial, to initiate blood coagulation. No fiber was

kept as control (Acontrol). The blood coagulation reaction was allowed to proceed at room temperature for 15 min. Following incubation, the clot and residual blood were carefully transferred into a Petri dish containing 25 mL of distilled water. The Petri dish with the blood clot solution was shaken for 10 min at 4 k rpm to release any residual hemoglobin. The absorbance of the resulting solution (Atest) was measured using a BioTek Synergy H1 multimode reader at 540 nm to assess the heam content in the solution [40]. The blood clotting index (%) is calculated using the equation below.

$$\text{Blood clotting index (\%)} = \frac{A_{test}}{A_{Control}} \times 100$$

3. Results and discussion

The concept of the waterfall theory of blood coagulation provided a foundational understanding of endogenous coagulation pathways, leading to the development of hemostatic agents that promote blood clotting by specifically targeting components within this cascade [41,42]. In recent years, biodegradable polysaccharides have gained significant attention for their unique physicochemical and biological properties, particularly in wound healing and tissue engineering. Studies have demonstrated that composite materials combining pullulan with other polymers exhibit enhanced structural and biological attributes, making them promising candidates for advanced wound dressings and drug delivery systems [32,43]. Pullulan plays a crucial role in the wound healing process, as it serves as an energy source for fibroblast cells that are essential for tissue regeneration [44,45]. Moreover, its hygroscopic nature accelerates wound closure and reduces healing time by promoting bacterial dehydration, effectively inactivating pathogens and minimizing their presence at the wound site. Additionally, by facilitating the dehydration of wound exudate, pullulan enhances cellular oxygenation, thereby creating a favorable environment for tissue repair and regeneration.

3.1. Fiber production

Initial attempts to produce Pull-Chi fibers at room temperature were successful. The lowest Chi concentration, <6 % Chi could not expel enough polymer mixture out of the spinneret at 14 k rpm for 10 min of rotation. Typically, 30G type needles with narrow internal diameter (0.159 mm) are recommended for fine fiber production [46]. However, in this work, 27G type needles with a larger internal diameter (0.210 mm) were necessary to facilitate the higher viscosity and cohesive forces of the Pull-Chi formulations out of the spinneret. Pure Pull fibers were also produced at room temperature using 27G type needles. However, the high viscosity and cohesive forces of Pull-Chi restricted their flow through the needles under the spinning system's energy conditions. To overcome this limitation, viscosity reduction was achieved by increasing the solution temperature. Temperatures between 45 and 65 °C were not sufficient to produce fibers, while temperatures close to or above 100 °C produced solution degradation by solvent evaporation and physical appearance transformation of the mixtures. However, the optimal temperature was determined to be 85 ± 2 °C for 25 min. Under these conditions, successful production of fibers wer obtainted (Fig. 3), and the production yield percentages were calculated. The optimized experimental conditions (rotation time, velocity, temperature, and concentrations) enabled fiber production within the first 5 min of spinning speeds of 7 k rpm for 6 % and 9 k rpm for Chi formulations, respectively.

3.2. Pull-Chi fiber production yields

The limited scalability of nanofiber production has been a significant challenge in the advancement and commercialization of electrospinning technologies, particularly when the fabrication of aligned nanofibers is required. The Pull-Chi fiber production yield curves are shown in Fig. 4. Both 6 % and 7 % Chi based formulations were capable of producing fibers. However, the 6 % Chi formulation consistently exhibited higher yields across the rotational speed range (6 k–14 k rpm) compared to 7 % Chi based formulations. The fiber yield increased with an increasing rotational speed, except for the 7 % sample that showed a decrease after 13 k rpm. The highest yield of around 90 % and 65 % was achieved for 6 % and 7 % Chi formulation. The reason for the difference in yield of fiber production is due to variation in solution viscosity, which in turn affects the mixture fluidities, and their ability to exit the spinneret to produce the fibrous material. Recent studies have highlighted centrifugal spinning as a promising alternative to electrospinning, offering higher productivity and improved process efficiency. This study demonstrates that centrifugal spinning enables the fabrication of uniform nanofibers with high yield [11]. Furthermore, advancements in centrifugal spinning technology have led to the development of high-throughput systems capable of generating large quantities of highly aligned nanofibers with tunable diameters, making it a viable approach for large-scale nanofiber production [17].

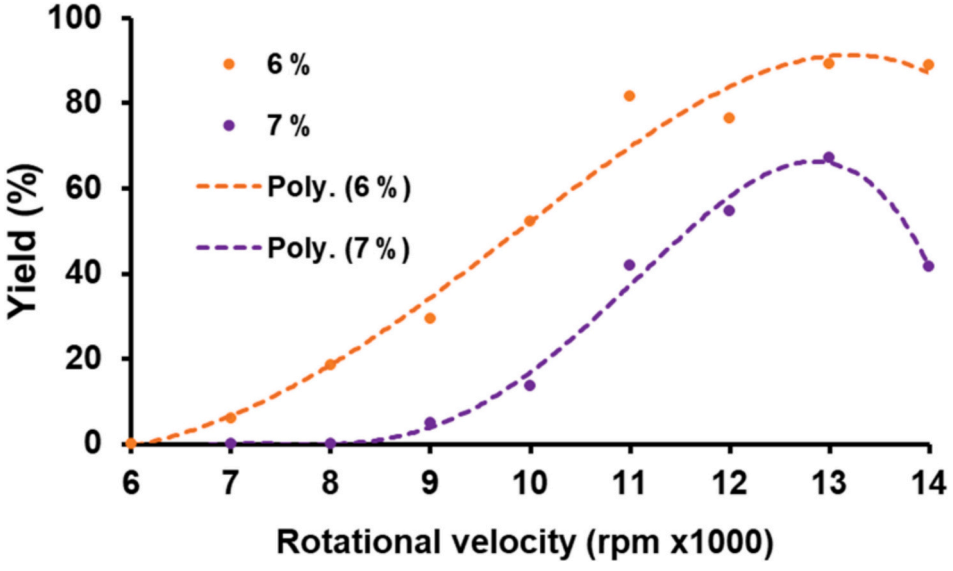

Fig. 4. Fiber production yields based on pullulan (15 %) and chitosan (6 % and 7 % of the solution) produced at different rotational speeds (rpm).

3.3. Fiber morphological analysis

The morphologies of the fibers were characterized using SEM and are presented in Figs. 5–6**.** The samples analyzed correspond to the fibers produced at 10 k rpm and 14 k rpm. The SEM micrographs revealed that polymer agglomerations, bead-like structures are observed along the fibers. Upon closer inspection at magnification of 150× demonstrates that the beads are neither oval nor spherical but rather present several morphologies in the mats. Notably, pull fibers produced at 10 k rpm do not display significant bead formation, indicating a more uniform fiber morphology. The Pull fibers are characterized by beads smaller than 40 μm, while the Pull-Chi fibers exhibit larger beads approximately 100 μm wide and >200 μm long. These morphological differences suggest that the incorporation of Chi into the Pull matrix significantly influences bead formation, due to changes in solution viscosity, surface tension, and polymer interactions. The presence of beads within the fiber matrix can introduce structural weaknesses, compromising the mechanical integrity of the material [47]. This reduction in structural stability may hinder its ability to provide adequate support for clot formation. Furthermore, beads can encapsulate biological agents or cause their localized accumulation, rather than ensuring their uniform distribution throughout the material, which may impact the overall efficacy of the

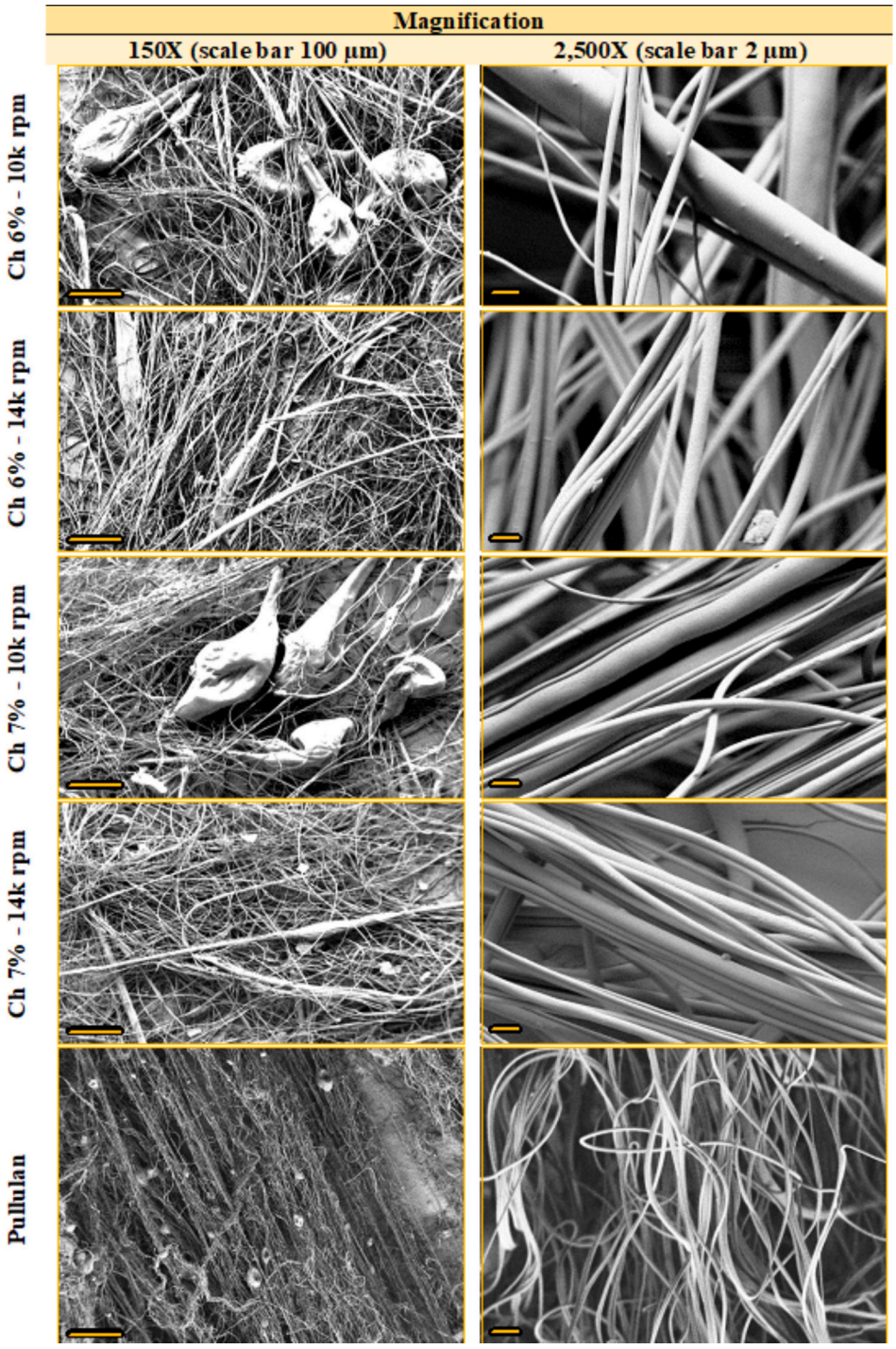

Fig. 5. SEM images of the fibers produced at different rpm, starting from solutions of pullulan (15 %) and chitosan at 6 % and 7 % in their composition. SEM of pure pullulan fibers obtained at 10 k rpm are shown at the bottom.

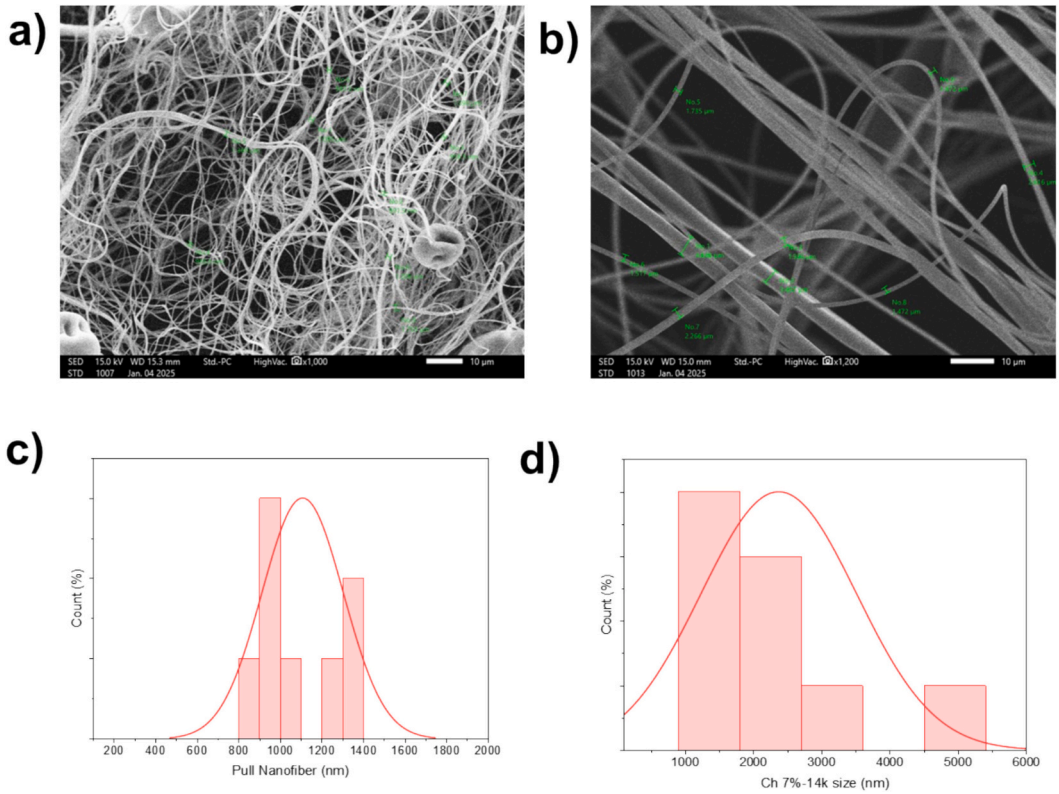

Fig. 6. SEM images of the fibers produced with (a) pullulan, (b) Pull- Chi 7 %, and (c-d) their respective nanofiber size histograms.

system [47–49]. Another notable difference is the fiber diameters. Pull fibers exhibit smaller diameters compared to Pull-Chi fibers, further corroborating the incorporation of the additive on the final material morphology. The increased fiber diameters in Pull-Chi systems can be attributed to the higher viscosity and cohesive forces introduced by the chitosan component, which impede the stretching and thinning of the polymer jet during the spinning process. The Pull fibers also shown in Fig. 5 correspond to a 10 k rpm test, this morphology is quite similar to the same composition fibers obtained at 14,000 rpm, whose most significant variation is a slight decrease in the number of beads with increasing of rotational speed.

On the other hand, as in the case of Pull fiber, composite mats decrease the number of beads and their sizes as the rotational speed increases**.** This effect is quite notable in fiber produced at 14 k rpm, which shows smaller quantity/size and more elongated beads than those obtained at 10 k rpm. This is due to the greater elongation that occurs in the fiber due to the greater kinetic energy with which the polymer jet (or mixture) is expelled out of the spinneret. The FDD analysis was performed using all the 2500× magnification micrographs shown in Figs. 5–6. Over 400 measurements were taken for each statistical analysis. The distribution curves results are presented in Fig. 7.

The general fiber diameter distribution (FDD) profiles (see Fig. 7a) demonstrate that the fibers containing Chi exhibit larger diameters compared to Pull fibers produced under the same experimental conditions. However, the Pull fibers consistently presented diameters within the nanometric scale. Since the Pull concentration remained kept constant, the addition of Chi increased the formulation viscosities, limiting the fibers elongation during the spinning process. These results indicate a direct proportional to the fiber diameter and Chi concentration in the formulations. A narrow diameter distribution can be obtained by increasing the rotational speed of the same formulation (see Fig. 7b). If the rotational speed is kept constant, then a broader diameter

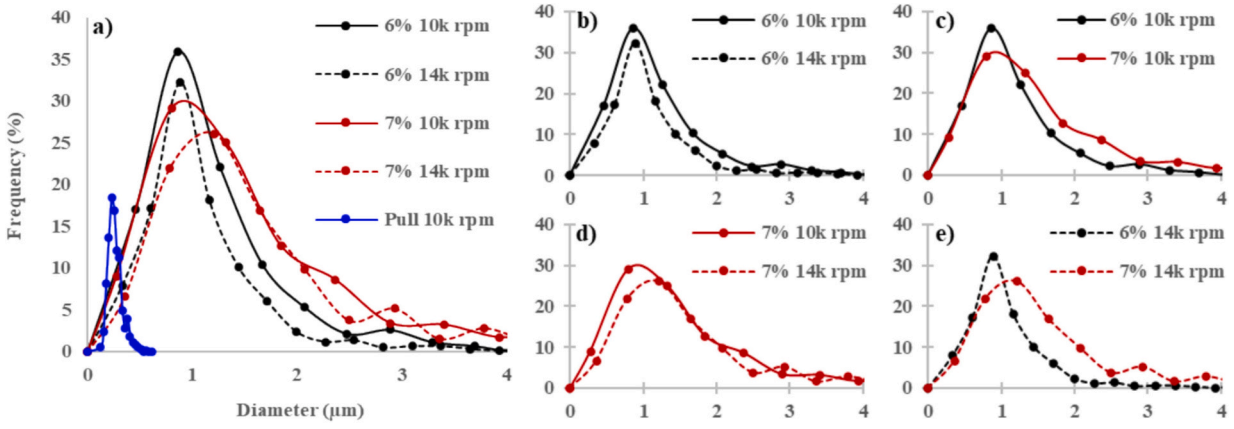

Fig. 7. FDD analysis of the Pull and Pull-Chi fibers produced by rotational spinning at different rpm. All X axes correspond to diameters between 0 and 4 μm.

distribution can be obtained by increasing the Chi concentration (see 7c, e). Finally, the Chi concentration can become so high in the formulations that the use of different rotational speeds does not exert a clear or significant effect on the fiber diameters (see 7d), since the cohesive forces of the mixtures are not so easily overcome by the centrifugal forces achieved in the spinning system. The percentage of fibers in the nano and micro scale for the developed systems is presented in Fig. 8.

This image indicates that the greater the Chi incorporation in the precursor formulations, the greater the diameter of the fibers produced. Pull fibers produced at velocities >10 k rpm (not included in the document) also presented nanometric diameters. This relationship directly impacts the possible applications of the materials since it affects both the mats permeabilities and the surface area. It is important to know the fiber mechanical characteristics and how they could be controlled, to determine the optimal formulation and/or production parameters according to the specific requirements of the product.

3.4. EDS analysis

The polymers used in this study are polysaccharides with distinct chemical compositions that allow for easy differentiation. Chitosan contains nitrogen (N) atoms as substituents within the amino functional groups, a characteristic feature of its molecular structure [50,51], while pullulan is solely composed of carbon (C), hydrogen (H), and oxygen (O) atoms [35,52] (Fig. 9). The EDA characterization results are presented as weight percent.

Fig. 9 illustrates theoretical atomic composition of pullulan with C and O accounting for approximately 59.5 % and 40.5 %, respectively, based on its molecular structure. These values align closely with the elemental chemical analysis, considering the associated margin of error and the lack of pre-treatment to remove surface contaminants (example O_2, CO, CO_2, or H_2O). H was not reported as the analysis focused on the elements C, O, and N for surface quantification. Based on these results, the EDS Pull-Chi fibers analysis confirms the presence of nitrogen confirming the successful integration of Chi into the Pull matrix. Nitrogen, present as amine groups, enhances the bioactivity of the composite by facilitating interactions with cells and proteins. These interactions play a crucial role in cell adhesion, which is essential for wound healing applications. Additionally, the nitrogen-containing functional groups contribute to the hemostatic properties of the fibers, as the positively charged amine groups can effectively interact with negatively charged erythrocytes, promoting coagulation and blood clot formation [53]. These values reflect both the atomic proportions of Chi and its concentration in the formulation. Notably, the nitrogen percentage of the 6 % Chi fibers slightly exceeded theoretical value, while the 7 % Chi fibers showed a marginal low value. Despite these differences, both results closely match theoretical expectations.

3.5. Thermogravimetric analysis

Thermogravimetric analyses and differential thermal analyses of the pure polymers and the composite fibers are presented in Fig. 10, detailing mass loss percentages and thermal behavior for each sample. All materials exhibit two distinct mass loss events at a well-defined temperature ranges. The first mass loss occurred below 100 °C, corresponding to dehydration, involving desorption of water molecules and evaporation of retained solvents within the fibers. The second mass loss, observed between 250 and 350 °C, is attributed to the thermal degradation of the polymeric components. Pullulan exhibits higher thermal stability than chitosan, and the Pull-Chi composite samples showed a slight decrease in thermal stability, which may be attributed to intermolecular hydrogen bonding interactions between the two polymers (see the FTIR section) These intermolecular interactions can disrupt the native packing and crystallinity of each polymer, making the material less thermally stable and causing an earlier onset of degradation. These degradation temperatures are consistent across raw materials and composite fibers and align with the literature reports for pullulan and chitosan [15,54]. The TGA results reveal significant differences in carbonaceous residue levels between 340 and 800 °C. The Chi sample produced 30.8 % residue, while Pull produced only 11.3 %, indicating higher stability for Chi. The composite fibers composed of 6 % and 7 % of Chi yielded residues of 18.6 and 21.1 % respectively, proportionally reflecting the residue behavior of the raw materials. The DTG analysis showed a maximum degradation temperature (MDT) of 300 °C for Chi and 320 °C for Pull. The composite fibers present an MDT around 317 °C, suggesting effective integration of Chi and Pull within the fibers. This intermediate thermal behavior indicates a strong compatibility between the polymer components. Finally, fibers fabricated at different rotational speeds but with identical Chi concentrations demonstrated no significant variation in their thermograms, highlighting the stability of thermal properties regardless of spinning conditions.

3.6. FT-IR spectral studies

The FTIR spectra of pullulan, chitosan, and pull-chi nanofibers are presented in Fig. 11. The FTIR spectrum of pure chitosan indicated a strong absorption broad band in the region of 3000 to 3600 cm^{-1}, corresponding to the stretching vibrations of -OH and -NH groups.

The peak at 2867 cm^{-1} was assigned to the stretching vibrations of -CH group. The peaks at 1033 and 1423 cm^{-1} belonged to C—O and -OH groups, respectively. The shoulder peak at 1644 cm^{-1} was attributed to C═O stretching vibration of amide I and the peak located at 1423 cm^{-1} corresponded to N—H bending of amide II. In the spectrum of pullulan, an absorption peak at 3292 cm^{-1} was due to the -OH stretching vibration and at 2906 cm^{-1} corresponded to the sp3 -CH stretching vibration. The single peak at 1644 cm^{-1} denoted the stretching vibration of O-C-O.

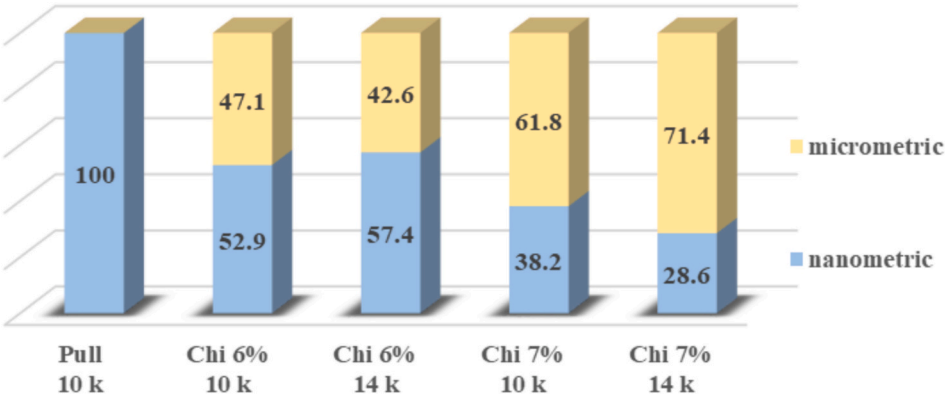

Fig. 8. Micro/nano-metric diameters proportions of the fibers produced at different rpm and with different Chi incorporations.

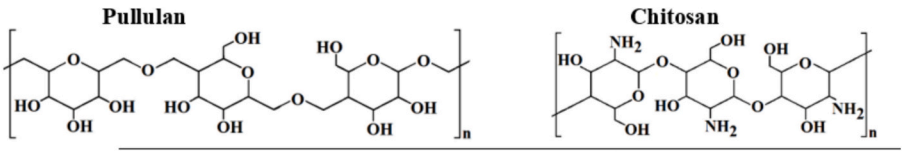

Surface atomic composition of the fibers (%)

Element	Pull		Pull-Chi (6 wt.%)		Pull-Chi (7 wt.%)	
	EDS	Theo	EDS	Theo	EDS	Theo
Carbon	57.3 ± 3.4	59.5	60.8 ± 2.3	58.5	61.0 ±2.3	58.4
Nitrogen	-	-	2.9 ± 0.6	2.7	2.7 ± 0.8	3.0
Oxygen	42.7 ± 4.7	40.5	36.3 ± 3.0	38.8	36.3 ± 3.0	38.6

Fig. 9. Molecular structures of the Pullulan and Chitosan basic polymerization units. Elemental chemical analysis performed by EDS of the Pull-Chi fibers produced by rotational spinning.

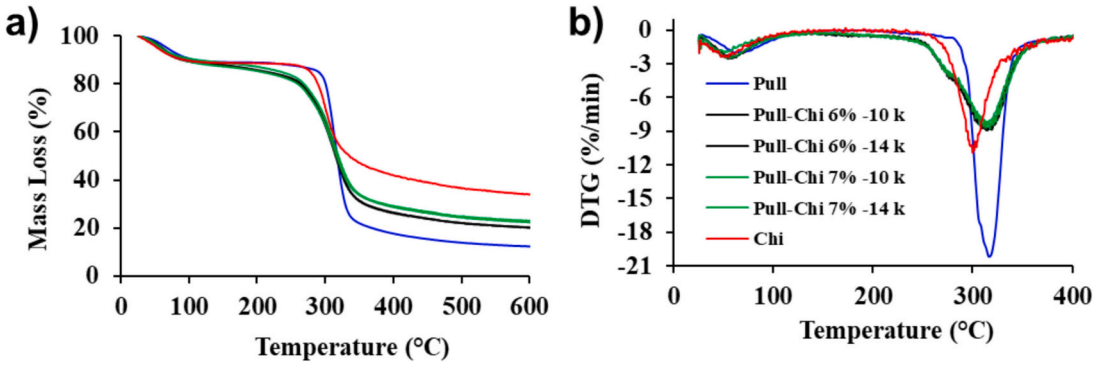

Fig. 10. Thermal properties of nanofibers. (a) Thermogravimetric and (b) differential thermal analyses of pure pullulan, chitosan, and composite Pull-Chi fibers produced by rotational spinning.

The broad absorption band between 3000 and 3600 cm^{-1} observed in the mixed chitosan and pullulan was associated with intermolecular hydrogen bonding between the hydroxy groups present in pullulan and the amino groups of chitosan. Furthermore, the peaks between 2855 and 2984 cm^{-1} and 1612–1687 cm^{-1} were ascribed to CH stretch vibrations of chitosan and pullulan, and the intermolecular hydrogen bond interaction of the -OH groups in pullulan and the amino group of chitosan (amide 1). The FTIR analysis demonstrated the presence of strong intermolecular hydrogen bond interaction between the amino groups of chitosan and the hydroxy groups of pullulan [55]. The final component proportions of the pullulan and chitosan formulations are presented in Table 1.

3.7. X-ray diffraction and contact angle measurement analyses

X-ray diffraction (XRD) analysis confirmed the structural characteristics of pullulan and pull-chi (7 %) nanofibers. The XRD pattern of pure pullulan film exhibited a broad diffraction peak at $2\theta = 10°$-$20°$, confirming its amorphous structure Fig. 12(a). The disappearance of the strong characteristic diffraction peaks of pullulan in the pull-chi nanofiber indicates significant structural modification. This transformation is primarily attributed to the formation of strong hydrogen bonds between chitosan and pullulan, which disrupts the original crystalline structure of pullulan within the nanofiber matrix. The surface wettability of nanofiber films was characterized by water contact angle (WCA) measurement and the results were illustrated in Fig. 12(b). The results revealed that pullulan nanofiber and pull-chi (6 % and 7 %) exhibited a WCA of 0°, confirming their high hydrophilicity. These findings are consistent with the observations of Abbasi et al., [56] reported an increase in WCA upon incorporating cellulose acetate into gelatin/cellulose acetate composite nanofiber films [56].

3.8. Rheology of Pull-Chi polymer blend solutions

The spinnability of a polymer solution is governed by the interplay of molecular entanglement, viscosity, surface tension, and conductivity. Fig. 13 presents the viscosity profiles of polymer solutions containing varying concentrations of pull-chi nanofibers at 6 and 7 %, respectively. The observed shear-thinning behavior is likely attributed to the disruption of the entangled polymer network and the breakdown of molecular interactions within the pull-chi dispersion as shear rate increases. At higher shear rates, the rate of intermolecular entanglement breakdown surpasses the rate of reformation, resulting in a gradual reduction in intermolecular resistance. Once the shear rate reaches a critical threshold, the viscosity stabilizes, indicating a complete disentanglement of polymer chains. Additionally, the apparent viscosity of the spinning dispersion decreased at lower chitosan concentrations within a specific shear rate range. This trend is consistent with previous reports and may be attributed to chitosan's ability to enhance hydrogen bonding interactions within the pull-chi dispersion, thereby influencing its rheological properties. Furthermore, Fig. 13(b) illustrates that the viscosity of the polymer solution increases with higher polymer concentrations at a fixed shear rate. These findings suggest that pull-chi solutions within the studied concentration range can effectively form continuous nanofibers, making them suitable for nanofiber fabrication.

3.9. Viscoelastic property of pull-chi nanofibers

Dynamic Mechanical Analysis (DMA) is a sensitive technique for studying how the viscoelastic properties of polymers change as a function of the thermal environment. Fig. 14 shows the measurement results of DMA at 1 Hz. The storage modulus decreases with the increase in temperature, and the loss modulus increases first and then decreases. If the storage modulus is greater than the loss modulus, then the material

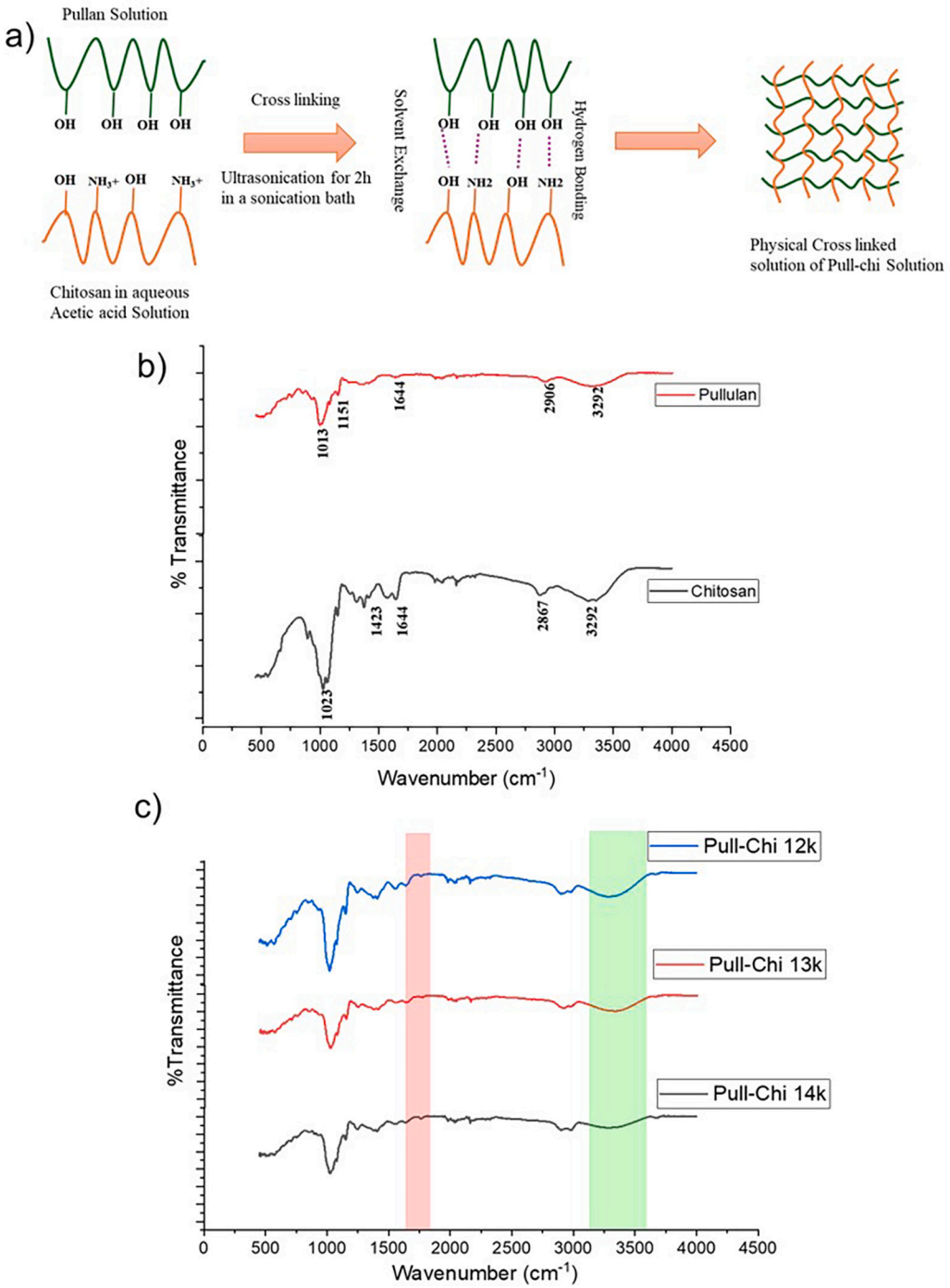

Fig. 11. Chemical composition analysis of nanofibers. (a) Schematic representation of physically crosslinked chitosan/pullulan nanofiber. The scheme is prepared considering reference [55]. (b-c) FTIR spectra of chitosan and pullulan and pull-chi (7 %) nanofiber of different batches.

can be regarded as mainly elastic. Conversely, if the loss modulus is greater than the storage modulus, then the material is predominantly viscous (it will dissipate more energy than it can store, like a flowing liquid). Since any polymeric material will exhibit both storage and loss modulus, they are termed as viscoelastic, and the measurements on the DMA are termed viscoelastic measurements. For a crosslinked polymer, the storage modulus value in the rubbery plateau region is correlated with the number of crosslinks in the polymer chain. The effects of crosslinking are clearly observed in the glass transition region as well as the rubbery plateau region [57,58].

3.10. Hemocompatibility of Pull-Chi fibers

Hemocompatibility is considered as a fundamental aspect in assessing biological and medical applications of nanofibers. It can be assessed through a hemolytic assay, which quantifies the release of free hemoglobin resulting from erythrocyte swelling and membrane rupture when red blood cells are exposed to materials being tested. In this study, the hemocompatibility of Pull-Chi fibers was evaluated using hemolysis assay (Fig. 15). PBS and Triton X-100 served as negative and positive control groups, respectively. The supernatants of the Pull-Chi fibers groups displayed a light red color similar to the PBS-negative control group, indicating minimal hemolysis. In contrast, 0.1 % Triton X

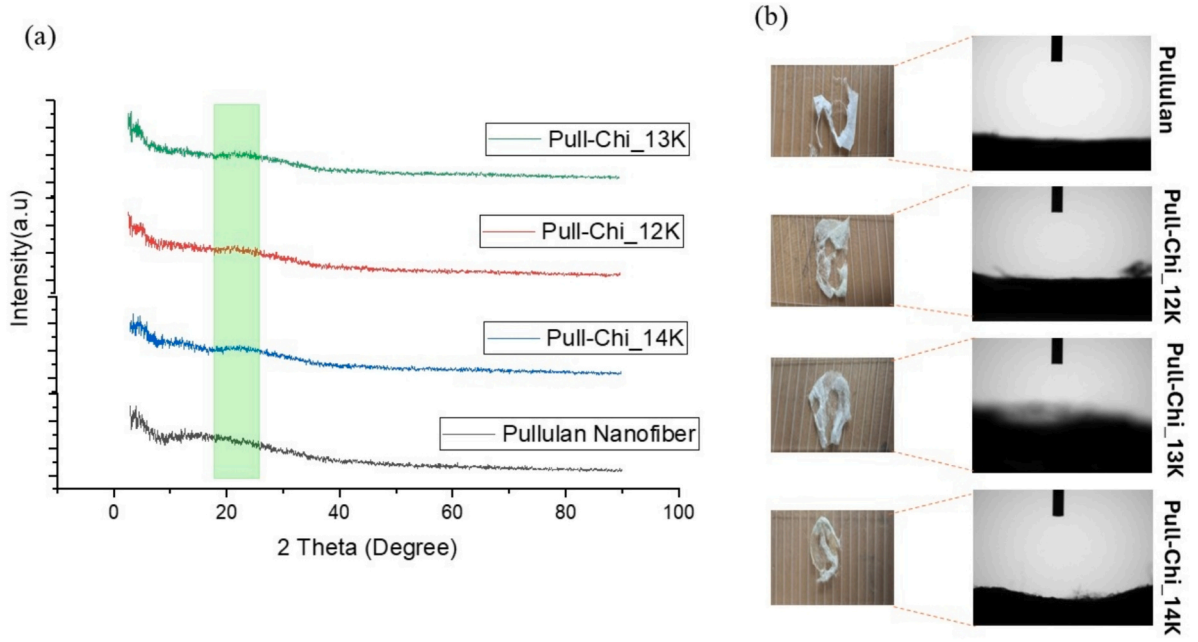

Fig. 12. X-ray diffraction and contact angle measurement analyses of nanofibers. (a) XRD patterns of pullulan and pull-chi (7 %) nanofibers and (b) contact angle and nanofiber evaluation of different pull-chi (6 and 7 %) nanofibers.

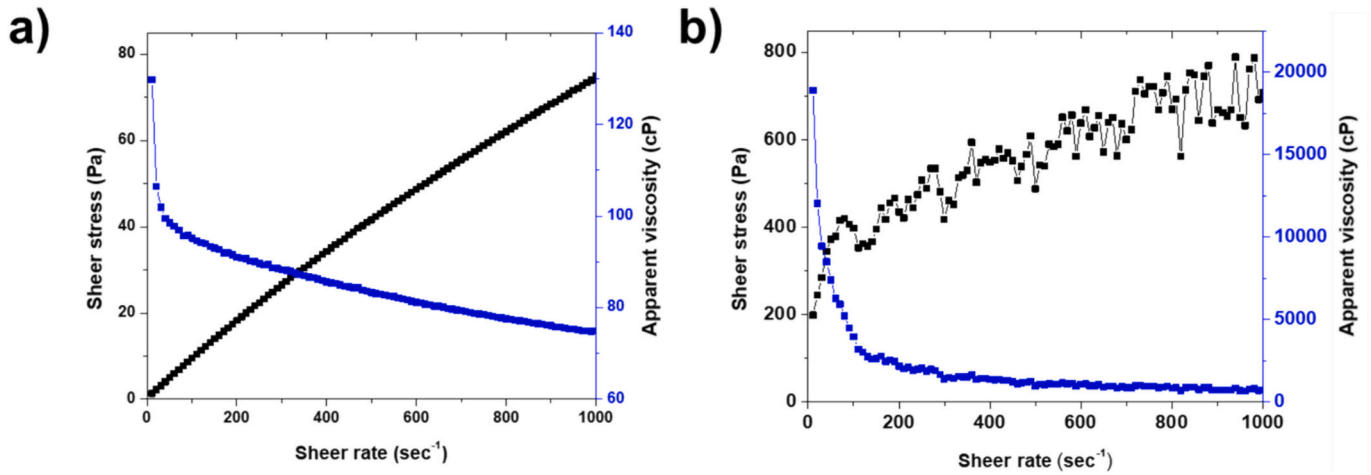

Fig. 13. Viscosity curves show the shear-thinning behavior for (a) Pull and (b) Pull-chi (7 %) blended solutions obtained using a rotational cone-plate measuring system.

resulted in a bright red supernatant, indicative of significant hemolysis, which was considered as 100 % hemolysis **(**Fig. 15 **a, purple bar).** Pull-Ch 7 %-14 k and pullulan fibers demonstrated hemolysis <1 % **(**Fig. 15 **a, red and green bars),** classifying them as hemocompatible based on American Society of Testing and Materials ASTM F756 [59], which defines hemolytic activity <5 % is considered as non-hemolytic. In addition, microscopic examination of RBCs treated with pullulan and Ch-7 %-14 k fibers revealed intact membranes, comparable to those in PBS-negative control treated group. In contrast, RBCs exposed to Triton X-100 exhibited complete cell rupture and loss of all cells (Fig. 15 b). These results conclusively demonstrate that Pull-Chi fibers, particularly the Ch-7 %-14 k formulation, exhibit excellent hemocompatibility, underscoring their potential for safe biomedical applications. RBCs constitute the most abundant cellular component of the bloodstream and play a critical role in determining hemocompatibility. Upon lysis, RBCs release hemoglobin along with procoagulant factors, which can trigger adverse physiological responses and potentially lead to complications such as thrombosis [60]. Damage to erythrocytes can compromise oxygen transport, reducing oxygen delivery to tissues and organs. Additionally, the release of erythrocyte-derived microvesicles has been shown to promote thrombus formation, further exacerbating circulatory disturbances and increasing the risk of vascular complications [61].

3.11. Coagulation tests

The hemostatic performance of Pull-Chi fibers was evaluated using a whole blood clotting index (BCI) assay, which measures the extent of red blood cell (RBC) aggregation within blood clots. Representative blood clotting images for the control group and treatment groups, including pullulan and Pull-Ch7%-14 k fibers, are shown in Fig. 16(a). The BCI indicates the proportion of unbound RBCs remaining outside the blood clot. Lower BCI values correspond to enhanced hemostatic capacity. The control group displayed poor RBC aggregation, with minimal

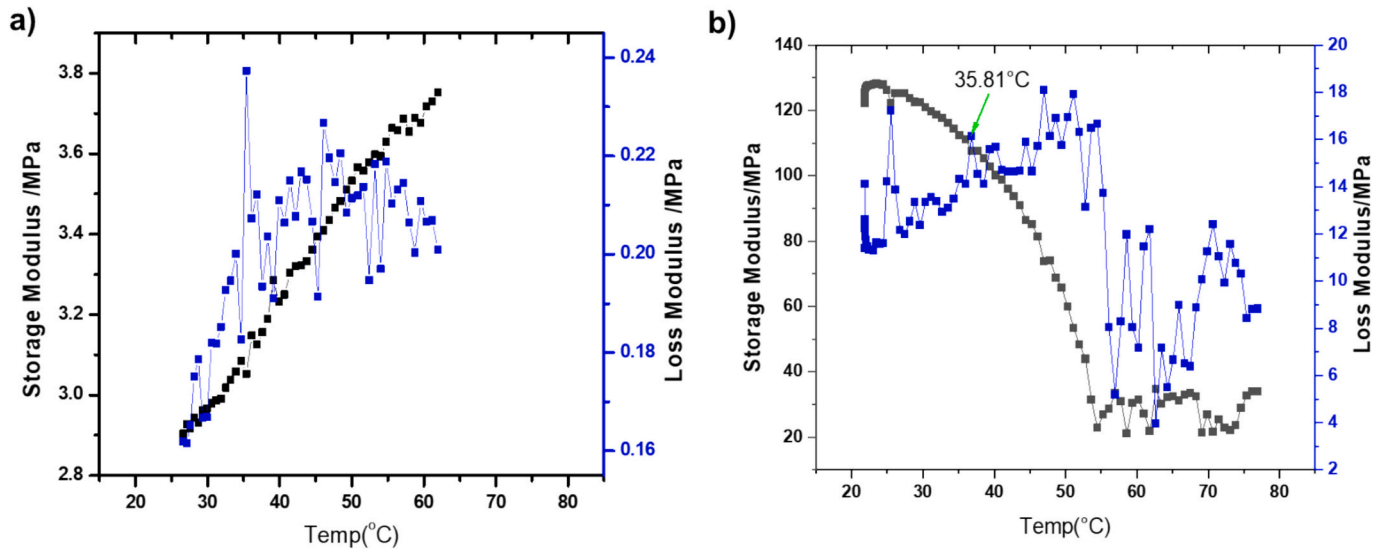

Fig. 14. Storage modulus and loss modulus vs. temperature curves for (a) Pull fiber and (b) Pull-Chi (7 %) obtained from DMA measurement.

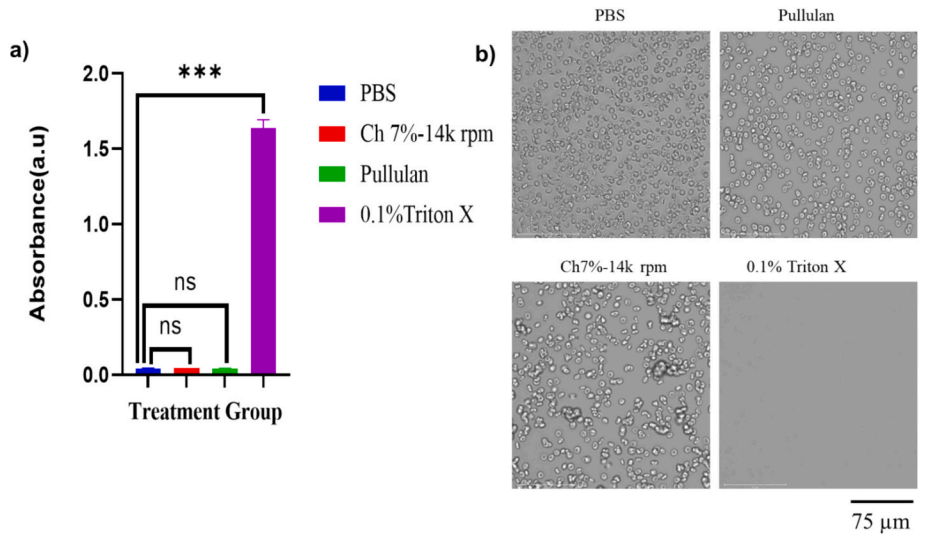

Fig. 15. The hemolysis assay of Pull-Chi fibers. (a) The hemolysis ratio of pullulan and Ch7%-14 k rpm fibers and control treatment groups (PBS, negative control and 1wt%Triton X, positive control). (b) Fibers indicated good hemocompatibility with <1 % hemolysis. The data represent the mean ± SD ($n = 5$), *** represents a significant difference, $p < 0.005$. Optical images of red blood cells after treatment with PBS, pullulan, Ch7%-14 k rpm, or a positive control (0.1 %) Triton X (2 mg). No significant morphological changes in pullulan and Ch7%-14 k rpm fibers, while few aggregations in Ch7%-14 rpm fibers compared to PBS. 0.1 % Triton X treated RBCs had completely vanished or lysed.

incorporation of RBCs into the clot, as evidenced by the lack of visual trapping (Fig. 16 (b)). In contrast, both pullulan and Pull-Ch7%-14 k fibers present a significant RBCs trapping within blood clots, indicated by white arrows, indicates a superior hemostatic performance of fibers. In addition, quantitative absorbance measurements further confirmed the enhanced hemostatic properties of pullulan and Pull-Chi fibers. The BCI values for pullulan and Pull-Ch7%-14krpm fibers were 51.51 ± 2.60 % and 65.43 ± 5.061 %, respectively, demonstrating significantly higher blood clot formation compared to the control group throughout the experiment (Fig. 16(c)).

These results are consistent with a previous study where chitosan, pullulan, and citric acid-based constructed nanofiber sponges achieved BCI value (~62 %), which is closely aligning with the Pull-Ch7%-14 k fibers in this study [40]. These findings indicate that Pull-Chi fibers, particularly the Pull-Ch7%-14 k formulation, exhibit enhanced hemostatic potential, surpassing pullulan fibers in promoting RBC aggregation and initiating effective blood clotting. This highlights the suitability of Pull-Chi fibers for advanced hemostatic applications. The von Willebrand factor (VWF) is a crucial glycoprotein involved in blood clotting, particularly under high shear rates. Structurally, it resembles a complex homopolymer, consisting of a repeating sequence of up to 100 functional monomeric units. VWF functions as a stimuli-responsive adhesive, remaining non-sticky and soluble in its inactive state. However, upon vascular injury, it undergoes chemical and mechanical activation, transforming into one of the strongest biological adhesives, facilitating rapid adhesion to both the injured substrate and platelets, thereby initiating the coagulation cascade [62]. Similarly, recent studies have demonstrated that porous pullulan-based hemostatic sponges exhibit remarkable mechanical properties. These properties are primarily attributed to the cross-linking of aldehyde groups with the hydroxyl groups of pullulan, enhancing the structural integrity and mechanical strength of the sponge, making it highly effective for hemostatic application [43].

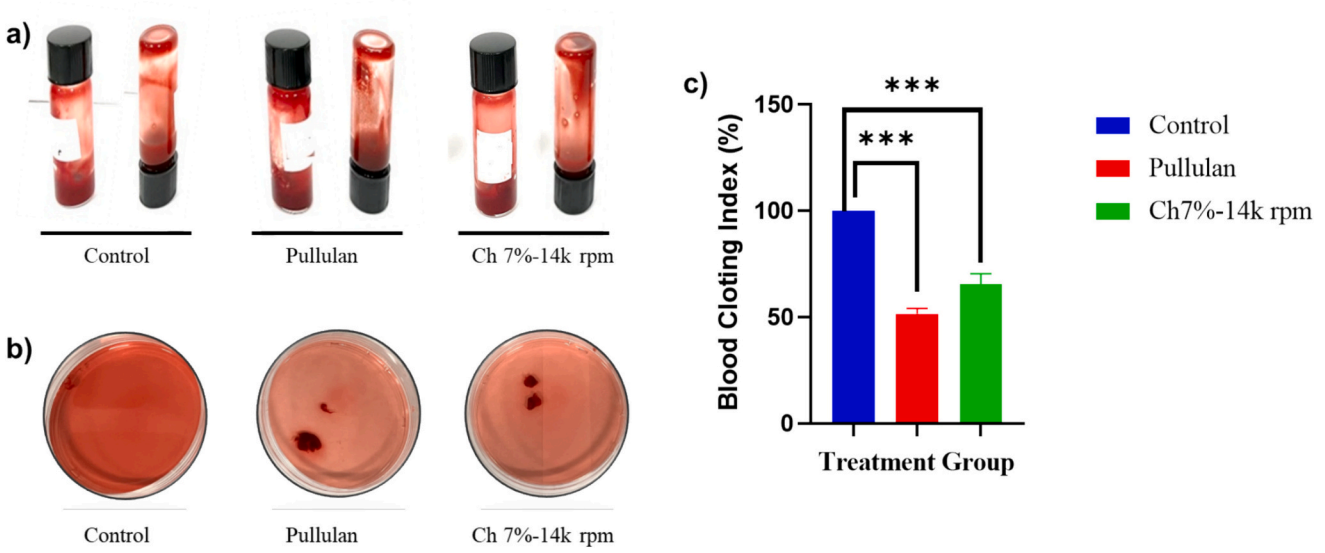

Fig. 16. The whole-blood clotting assay of Pull-Chi fibers. (a) The representative images of control and treatment samples in blood clotting index study. (b) Blood clotting index visualization of RBC entrapment in blood clots, and (c) the absorbance value negatively correlated with blood clot formation, which was reflected by the blood-clotting index (%). The pullulan and ch7%-14 k rpm fiber treatment group showed a significantly lower BCI than that of control group. The data represent the mean ± SD ($n = 3$), *** represents a significant difference, $p < 0.005$.

4. Conclusions

Uncontrolled bleeding, whether resulting from injuries, trauma, surgical procedures, or hereditary and drug-induced coagulation disorders, presents significant health risks. Pullulan-based fibers were successfully fabricated using 15 % pullulan solution supplemented with chitosan concentrations of 6 % and 7 % in the aqueous precursor formulations. The production of fibers was facilitated by increasing the solution temperature and employing rotational spinning at speeds exceeding 7 k rpm. The optimal fiber yields of approximately 90 % and 65 % were at higher speed (13 k rpm) with the 6 % and 7 % Chi formulations, respectively. The morphological analysis indicates that the majority of fibers were within the nanometric scale. Higher rotational speeds were associated with a reduction in both the number and dimensions of bead-like structures along fibers, indicating improved fiber uniformity. In addition, the present study yielded several key findings: (i) Nanofiber characterization using FT-IR, PXRD, and contact angle measurements confirmed its amorphous nature and crosslinking interactions, (ii) Compared to a plain membrane, the nanofiber exhibited superior hydrophilicity, enhancing its potential for biomedical applications, (iii) The strong hydrogen bonding interactions between pullulan and chitosan significantly improved hydrophilicity and permeability, making the nanofiber a promising candidate for wound healing and hemostatic applications. An optimized Pull-Chi fibers exhibited hemocompatibility and significant hemostatic potential, making them promising candidates for biomedical applications. Further preclinical studies, including animal models, are necessary to evaluate their clinical translatability.

CRediT authorship contribution statement

Jefferson Reinoza: Writing – review & editing, Writing – original draft, Visualization, Validation, Resources, Methodology, Investigation, Formal analysis, Data curation, Conceptualization. **Rahul Tiwari:** Writing – review & editing, Writing – original draft, Visualization, Validation, Formal analysis, Data curation. **Isabela Morales:** Visualization, Validation, Methodology, Formal analysis, Data curation. **Luis Sotelo:** Visualization, Validation, Methodology, Formal analysis, Data curation. **Debabrata Sengupta:** Writing – review & editing, Writing – original draft, Visualization, Validation, Methodology, Investigation, Formal analysis, Data curation. **Juan Pablo Hernandez:** Writing – review & editing, Writing – original draft, Visualization, Validation, Methodology, Data curation. **Victoria Padilla:** Writing – review & editing, Writing – original draft, Visualization, Validation, Supervision, Software, Methodology, Investigation, Formal analysis, Data curation, Conceptualization. **Murali M. Yallapu:** Writing – review & editing, Writing – original draft, Supervision, Software, Resources, Project administration, Methodology, Funding acquisition, Formal analysis, Conceptualization. **Karen Lozano:** Writing – review & editing, Writing – original draft, Supervision, Software, Resources, Project administration, Methodology, Investigation, Funding acquisition, Formal analysis, Conceptualization.

Declaration of competing interest

The authors declare that they have no known competing financial interests or personal relationships that could have appeared to influence the work reported in this paper.

Acknowledgements

The authors gratefully acknowledge the support received by the National Science Foundation under PREM award DMR 2122178, NIH (U54MD019970/GM139727), and CPRIT (RP210180/RP230419).

Data availability

Data will be made available on request.

References

[1] N.T. Institute, available at https://www.nattrauma.org/trauma-statistics-facts/. Accessed on November, 2022.
[2] S.A. Tisherman, R.H. Schmicker, K.J. Brasel, E.M. Bulger, J.D. Kerby, J.P. Minei, J. L. Powell, D.A. Reiff, S.B. Rizoli, M.A. Schreiber, Detailed description of all deaths in both the shock and traumatic brain injury hypertonic saline trials of the resuscitation outcomes consortium, Ann. Surg. 261 (3) (2015) 586–590.
[3] R.K. Latif, S.P. Clifford, J.A. Baker, R. Lenhardt, M.Z. Haq, J. Huang, I. Farah, J. R. Businger, Traumatic hemorrhage and chain of survival, Scand. J. Trauma Resusc. Emerg. Med. 31 (1) (2023) 25.
[4] Y. Guo, M. Wang, Q. Liu, G. Liu, S. Wang, J. Li, Recent advances in the medical applications of hemostatic materials, Theranostics 13 (1) (2023) 161–196.

[5] R. Yadav, R. Kumar, M. Kathpalia, B. Ahmed, K. Dua, M. Gulati, S. Singh, P. J. Singh, S. Kumar, R.M. Shah, P.K. Deol, I.P. Kaur, Innovative approaches to wound healing: insights into interactive dressings and future directions, J. Mater. Chem. B 12 (33) (2024) 7977–8006.
[6] P. Yu, W. Zhong, Hemostatic materials in wound care, Burns trauma 9 (2021) tkab019.
[7] Z. Jiang, Z. Zheng, S. Yu, Y. Gao, J. Ma, L. Huang, L. Yang, Nanofiber scaffolds as drug delivery systems promoting wound healing, Pharmaceutics 15 (7) (2023) 1829.
[8] V. Kumar, N. Sharma, P. Janghu, R. Pasrija, M. Umesh, P. Chakraborty, S. Sarojini, J. Thomas, Synthesis and characterization of chitosan nanofibers for wound healing and drug delivery application, J. Drug Deliv. Sci. Technol. 87 (2023) 104858.
[9] C. Pang, K.S. Fan, L. Wei, M.K. Kolar, Gene therapy in wound healing using nanotechnology, Wound Repair Regen. 29 (2) (2021) 225–239.
[10] R.-X. Chen, Y. Li, J.-H. He, Mini-review on Bubbfil spinning process for mass-production of nanofibers, Matéria (Rio de Janeiro) 19 (4) (2014) 325–343.
[11] X. Zhang, Y. Lu, Centrifugal spinning: an alternative approach to fabricate nanofibers at high speed and low cost, Polym. Rev. 54 (4) (2014) 677–701.
[12] L. Zhou, S. Zhai, Y. Chen, Z. Xu, Anisotropic cellulose nanofibers/polyvinyl alcohol/graphene aerogels fabricated by directional freeze-drying as effective oil adsorbents, Polymers 11 (4) (2019) 712.
[13] D. Reneker, A. Yarin, E. Zussman, H. Xu, Electrospinning of nanofibers from polymer solutions and melts, Adv. Appl. Mech. 41 (2007) 43–346.
[14] C.A. Delgado, A. Chapa, K. Lozano, A. Fuentes, H. Vasquez, In-situ surface depositing of Nano–Micro-particles on electrospun fibers, Fibers Polym. 25 (2) (2024) 407–413.
[15] S. Ahmed, M. Keniry, V. Padilla, N. Anaya-Barbosa, M.N. Javed, R. Gilkerson, K. Gomez, A. Ashraf, A.S. Narula, K. Lozano, Development of pullulan/chitosan/salvianolic acid ternary fibrous membranes and their potential for chemotherapeutic applications, Int. J. Biol. Macromol. 250 (2023) 126187.
[16] M.A. Hammami, M. Krifa, O. Harzallah, Centrifugal force spinning of PA6 nanofibers–processability and morphology of solution-spun fibers, J. Text. Inst. 105 (6) (2014) 637–647.
[17] A.E. Erickson, D. Edmondson, F.-C. Chang, D. Wood, A. Gong, S.L. Levengood, M. Zhang, High-throughput and high-yield fabrication of uniaxially-aligned chitosan-based nanofibers by centrifugal electrospinning, Carbohydr. Polym. 134 (2015) 467–474.
[18] A. Sabir, F. Altaf, M. Shafiq, Synthesis and characterization and application of chitin and chitosan-based eco-friendly polymer composites, in: Sustainable polymer composites and nanocomposites, 2019, pp. 1365–1405.
[19] S. Zhang, X. Lei, Y. Lv, L. Wang, L.-N. Wang, Recent advances of chitosan as a hemostatic material: hemostatic mechanism, material design and prospective application, Carbohydr. Polym. 327 (2024) 121673.
[20] P. Fan, Y. Zeng, D. Zaldivar-Silva, L. Agüero, S. Wang, Chitosan-based hemostatic hydrogels: the concept, mechanism, application, and prospects, Molecules 28 (3) (2023) 1473.
[21] K. Ohkawa, K.-I. Minato, G. Kumagai, S. Hayashi, H. Yamamoto, Chitosan nanofiber, Biomacromolecules 7 (11) (2006) 3291–3294.
[22] V. Sencadas, D.M. Correia, A. Areias, G. Botelho, A. Fonseca, I. Neves, J.G. Ribelles, S.L. Mendez, Determination of the parameters affecting electrospun chitosan fiber size distribution and morphology, Carbohydr. Polym. 87 (2) (2012) 1295–1301.
[23] S. Mengistu Lemma, F. Bossard, M. Rinaudo, Preparation of pure and stable chitosan nanofibers by electrospinning in the presence of poly (ethylene oxide), Int. J. Mol. Sci. 17 (11) (2016) 1790.
[24] N. Ketabchi, M. Naghibzadeh, M. Adabi, S.S. Esnaashari, R. Faridi-Majidi, Preparation and optimization of chitosan/polyethylene oxide nanofiber diameter using artificial neural networks, Neural Comput. & Applic. 28 (2017) 3131–3143.
[25] K. Choo, Y.C. Ching, C.H. Chuah, S. Julai, N.-S. Liou, Preparation and characterization of polyvinyl alcohol-chitosan composite films reinforced with cellulose nanofiber, Materials 9 (8) (2016) 644.
[26] J. Xu, J. Zhang, W. Gao, H. Liang, H. Wang, J. Li, Preparation of chitosan/PLA blend micro/nanofibers by electrospinning, Mater. Lett. 63 (8) (2009) 658–660.
[27] X. Zhuang, B. Cheng, W. Kang, X. Xu, Electrospun chitosan/gelatin nanofibers containing silver nanoparticles, Carbohydr. Polym. 82 (2) (2010) 524–527.
[28] S.V.G. Nista, J. Bettini, L.H.I. Mei, Coaxial nanofibers of chitosan–alginate–PEO polycomplex obtained by electrospinning, Carbohydr. Polym. 127 (2015) 222–228.
[29] Z.-x. Cai, X.-m. Mo, K.-h. Zhang, L.-p. Fan, A.-l. Yin, C.-l. He, H.-s. Wang, Fabrication of chitosan/silk fibroin composite nanofibers for wound-dressing applications, Int. J. Mol. Sci. 11(9) (2010) 3529–3539.
[30] S. Tabasum, A. Noreen, M.F. Maqsood, H. Umar, N. Akram, Z.H. Nazil, S.A. S. Chatha, K.M. Zia, A review on versatile applications of blends and composites of pullulan with natural and synthetic polymers, Int. J. Mol. Sci. 120 (2018) 603–632.
[31] K. Kraśniewska, K. Pobiega, M. Gniewosz, Pullulan–biopolymer with potential for use as food packaging, De Gruyter 15 (9) (2019) 20190030.
[32] S. Agrawal, D. Budhwani, P. Gurjar, D. Telange, V.J.D.d. Lambole, Pullulan based derivatives: Synthesis, enhanced physicochemical properties, and applications, Drug Deliv. 29 (1) (2022) 3328–3339.
[33] Z. Qin, X. Jia, Q. Liu, B. Kong, H. Wang, Enhancing physical properties of chitosan/pullulan electrospinning nanofibers via green crosslinking strategies, Carbohydr. Polym. 247 (2020) 116734.
[34] G.N.N.G.U.F.a.D.A. Agency Response Letter, 2002).
[35] M.B. Coltelli, S. Danti, K. De Clerck, A. Lazzeri, P. Morganti, Pullulan for advanced sustainable body- and skin-contact applications, J. Funct. Biomater. 11 (1) (2020).
[36] A. Younas, Z. Dong, Z. Hou, M. Asad, M. Li, N. Zhang, A chitosan/fucoidan nanoparticle-loaded pullulan microneedle patch for differential drug release to promote wound healing, Carbohydr. Polym. 306 (2023) 120593.
[37] R.A. Ilyas, H.A. Aisyah, A.H. Nordin, N. Ngadi, M.Y.M. Zuhri, M.R.M. Asyraf, S. M. Sapuan, E.S. Zainudin, S. Sharma, H. Abral, M. Asrofi, E. Syafri, N.H. Sari, M. Rafidah, S.Z.S. Zakaria, M.R. Razman, N.A. Majid, Z. Ramli, A. Azmi, S. P. Bangar, R. Ibrahim, Natural-fiber-reinforced chitosan, chitosan blends and their nanocomposites for various advanced applications, Polymers 14 (5) (2022) 874.
[38] M.M. Yallapu, M.C. Ebeling, N. Chauhan, M. Jaggi, S.C. Chauhan, Interaction of curcumin nanoformulations with human plasma proteins and erythrocytes, Int. J. Nanomedicine 6 (2011) 2779–2790.
[39] Y. Gong, P. Chowdhury, P.K.B. Nagesh, M.A. Rahman, K. Zhi, M.M. Yallapu, S. Kumar, Novel elvitegravir nanoformulation for drug delivery across the blood-brain barrier to achieve HIV-1 suppression in the CNS macrophages, Sci. Rep. 10 (1) (2020) 3835.
[40] F. Jiang, Q. Li, Y. Li, X. Lai, Y. Duan, A. McDowell, Z. Huang, S. Liu, Y. Wang, C. Zhang, Y. Qu, X. Pan, 3D electrospun nanofiber sponges of insect chitosan/pullulan/citric acid embedded with ZnMOF in situ for enhanced healing of MRSA-infected wounds, Chem. Eng. J. 498 (2024) 155388.
[41] C. Hougie, The waterfall-cascade and autoprothrombin hypotheses of blood coagulation: personal reflections from an observer, J. Thromb. Haemost. 2 (8) (2004) 1225–1233.
[42] E.W. Davie, A brief historical review of the waterfall/cascade of blood coagulation, J. Biol. Chem. 278 (51) (2003) 50819–50832.
[43] W. Zheng, Z. Zhang, Y. Li, L. Wang, F. Fu, H. Diao, X. Liu, A novel pullulan oxidation approach to preparing a shape memory sponge with rapid reaction capability for massive hemorrhage, Chem. Eng. J. 447 (2022) 137482.
[44] R.S. Singh, N. Kaur, V. Rana, J.F. Kennedy, Recent insights on applications of pullulan in tissue engineering, Carbohydr. Polymer. 153 (2016) 455–462.
[45] M.O. Teixeira, E. Marinho, C. Silva, J.C. Antunes, H.P. Felgueiras, Technology, Pullulan hydrogels as drug release platforms in biomedicine, J. Drug Deliv. Sci. Technol. 89 (2023) 105066.
[46] C. Hernandez, S.K. Gupta, J.P. Zuniga, J. Vidal, R. Galvan, H. Guzman, L. Chavez, K. Lozano, Y. Mao, High pressure responsive luminescence of flexible Eu3+ doped PVDF fibrous mats, J. Mater. Sci. Technol. 66 (2021) 103–111.
[47] G. Sabarees, S. Vishvaja, S. Raghuraman, V. Velmurugan, V. Alagarsamy, V. Raja Solomon, G. Padmini Tamilarasi, Collagen-based nanofibers: revolutionizing therapeutics for impaired wound healing, international journal of polymeric materials and polymeric, Biomaterials (2024) 1–29.
[48] S.M.H. Marjuban, M. Rahman, S.S. Duza, M.B. Ahmed, D.K. Patel, M.S. Rahman, K. Lozano, Recent advances in centrifugal spinning and their applications in tissue engineering, Polymers 15 (5) (2023) 1253.
[49] M. Broadwin, F. Imarhia, A. Oh, C.R. Stone, F.W. Sellke, S. Bhowmick, M.R. Abid, Exploring electrospun scaffold innovations in cardiovascular therapy: a review of electrospinning in cardiovascular disease, Bioengineering 11 (3) (2024) 218.
[50] Hakima El Knidri, Ali Laajeb, A. Lahsini, Chapter 2 - Chitin and chitosan: chemistry, solubility, fiber formation, and their potential applications, in: Handbook of Chitin and Chitosan, Elsevier, 2020, pp. 35–57.
[51] S. Ahmed, M. Ahmad, S. Ikram, Chitosan: A natural antimicrobial agent-A review, J. Appl. Chem. 3 (2) (2014) 493–503.
[52] L. Ghimici, M. Constantin, A review of the use of pullulan derivatives in wastewater purification, React. Funct. Polym. 149 (2020) 104510.
[53] Y. Wan, J. Han, F. Cheng, X. Wang, H. Wang, Q. Song, W. He, Green preparation of hierarchically structured hemostatic epoxy-amine sponge, Chem. Eng. J. 397 (2020) 125445.
[54] F. Xu, B. Weng, R. Gilkerson, L.A. Materon, K. Lozano, Development of tannic acid/chitosan/pullulan composite nanofibers from aqueous solution for potential applications as wound dressing, Carbohydr. Polym. 115 (2015) 16–24.
[55] C.N. Elangwe, S.N. Morozkina, A.V. Podshivalov, M.V. Uspenskaya, Evaluation of composition effects on the tissue-adhesive, mechanical and physical properties of physically crosslinked hydrogels based on chitosan and pullulan for wound healing applications, Int. J. Biol. Macromol. 276 (2024) 133857.
[56] H. Abbasi, H. Fahim, M. Mahboubi, Fabrication and characterization of composite film based on gelatin and electrospun cellulose acetate fibers incorporating essential oil, J. Food Meas. Charact. 15 (2) (2021) 2108–2118.
[57] J. Sarina, L. Zhang, Zhang, Dynamic mechanical properties of *Eucommia ulmoides* gum with different degree of cross-linking, Polym. Bull. 68 (2012) 2021–2032.
[58] D. Kong, Y. Meng, G.B. McKenna, Determination of the molecular weight between cross-links for different ambers: viscoelastic measurements of the rubbery plateau, Polym. Eng. Sci. 62 (4) (2022) 1023–1040.
[59] P. ASTM. F 756–00: Standard Practice for Assessment of Hemolytic Properties of Materials. Annual Book of ASTM Standards; American Society of Testing and Materials: West Conshohocken.
[60] C. Kloypan, N. Suwannasom, S. Chaiwaree, A. Prapan, K. Smuda, N. Baisaeng, A. Pruß, R. Georgieva, H. Bäumler, In-vitro haemocompatibility of dextran-protein submicron particles, Artif. Cells Nanomed. Biotechnol. 47 (1) (2019) 241–249.
[61] I. Geremia, D. Pavlenko, K. Maksymow, M. Rüth, H. Lemke, D. Stamatialis, Ex vivo evaluation of the blood compatibility of mixed matrix haemodialysis membranes, Acta Biomater. 111 (2020) 118–128.
[62] A. Alexander-Katz, Toward novel polymer-based materials inspired in blood clotting, Macromolecules 47 (5) (2014) 1503–1513.